UNIVERSIDAD DE CANTABRIA

Facultad de Ciencias

Departamento de Física Aplicada

Tesis Doctoral

SYNTHESIS, STRUCTURAL CHARACTERIZATION AND SPECTROSCOPIC STUDY OF NANOCRYSTALLINE AND MICROCRYSTALLINE MATERIALS

Rosa Martín Rodríguez

Santander, Noviembre de 2010

Chapter 6

Semiconductor nanoparticles. Optical spectroscopy at high pressure

6.1 Introduction

In this chapter, we show the main results concerning optical spectroscopy of CdS and $Zn_{1-x}Co_xO$ nanoparticles at high pressure and the influence of pressure-induced phase transitions on these properties. The physical properties in the nanocrystal regime can be quite different from those of the bulk. For instance, there are many works which demonstrate a decrease in the melting temperature [1], [2], [3] as well as an increase of the transition pressure [4], [5] with decreasing nanoparticles size. This behavior may arise because of the relatively high energy surfaces in nanocrystals which make the high pressure phase less stable than in the bulk [4]. Besides, nanoparticles lack the internal defects that serve as nucleation points for structural phase transitions [6].

CdS is a well-studied II-VI semiconductor due to its many applications such as bio-labeling or light emitting diodes [7], [8]. The bulk crystallizes in the W structure while both W and RS structures have been found for CdS QDs [9]. The main interest in the study of its optical properties arises from the fact that they are size-dependent. Absorption, Raman and XRD measurements have been performed in this work in order to characterize the ZB-to-RS phase transition in CdS nanoparticles prepared by ball milling.

DMSs are currently attracting intense interest in different applied areas like the emerging field of spin-based electronics [10], [11]. Although TM^{2+}-doped ZnO DMSs have been

proposed to be favorable candidates for RT ferromagnetism, the magnetic behavior is extremely sensitive to the synthesis procedure and remains controversial [12], [13]. The magnetization measurements carried out by M. A. White *et al.* on W-$Zn_{1-x}Co_xO$ colloidal nanocrystals prepared following the same synthesis method as in this work, indicated a paramagnetic-like magnetism at low Co^{2+} concentrations and an antiferromagnetic behavior for W-CoO, with no ferromagnetic response [14]. In our case, Co^{2+} impurities have been used as a local probe to monitor the phase transition under high pressure in $Zn_{1-x}Co_xO$ nanocrystals. The RS-to-W phase transition has also been studied by means of bandgap absorption and Raman spectroscopy.

6.2 CdS nanoparticles

6.2.1 Synthesis and characterization

Depending on the particle size, different structures have been identified for CdS nanocrystals [9]. (i) When the size is smaller than 5 nm, CdS nanoparticles are mainly crystallized in the metastable cubic ZB structure (space group $F\bar{4}3m$). (ii) When the size is larger than about 8 nm, they are in the stable hexagonal W structure ($P6_3mc$ space group). (iii) In between, they are in intermediate phases. In both ZB and W structure each anion is surrounded by four cations at the corners of a tetrahedron and viceversa. These results have also been observed in the structural analysis of colloidal CdSe nanocrystals deduced from XRD by Bawendi *et al.* [15]. In bulk CdS crystals with the W structure, the $\Gamma_{15}^V \rightarrow \Gamma_1^C$ direct gap is the lowest in energy (E_g = 2.4 eV at 300 K) and indirect gaps occur at least 1 eV above E_g and always stay above E_g at high pressure [16]. Investigations of electronic structure in W- and ZB-CdS showed that the fundamental direct bandgaps in both structures differ by less than 0.1 eV [17]. Since the exciton Bohr radius in bulk CdS is 2.6 nm [18], CdS nanocrystals with the metastable ZB structure (diameter less or equal to 5 nm) are in the weak confinement regime. Therefore, the direct optical energy gaps of bulk and nanocrystals are similar.

Pure and Yb^{3+}-doped CdS nanocrystals have been prepared in a planetary ball mill as described in Section 3.2.3. These materials show an intense orange color. The initial idea

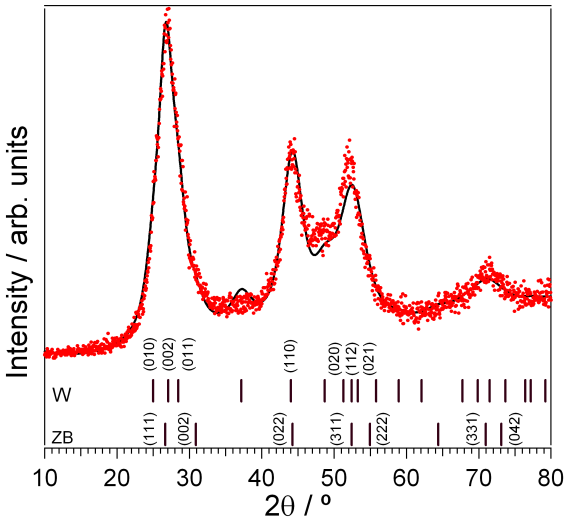

Figure 6.1: XRD pattern of the CdS nanocrystalline samples prepared by ball milling. The black line corresponds to the calculated pattern for the ZB-W mixed structure, and ticks indicate the (hkl) index for each crystallographic phase.

for this system was obtaining bandgap UC emission upon Yb^{3+} excitation. XRD pattern of CdS nanoparticles together with a Rietveld refinement considering both cubic and hexagonal phases is shown in Fig. 6.1. The best fitting for the prepared nanocrystalline sample is obtained for a 85% ZB - 15% W mixed structure; however, the error associated to this quantitative analysis is pretty large, and variations in some fitting parameters may lead the ZB contribution to a minimum value of 65%. The cell parameter obtained for the ZB phase, a=5.7844 Å, is slightly smaller than the bulk value, a_0=5.818 Å [19]. The values for the W structure, a=4.1111 Å and c=6.5837 Å, are somewhat different to those of the bulk (a_0=4.137 Å and c_0=6.7144 Å) [20]. The $\frac{c}{a}$(nano) = 1.60 and $\frac{c_0}{a_0}$(bulk) = 1.62 ratios give a 1% deviation from the bulk; this estimation of the W structure distortion is smaller than the up to 15% differences observed by Kumpf *et al.* [21].

The average particle size of the as-obtained nanoparticles, according to the Williamson-Hall equation (eq. 4.1), has been determined to be about 5 nm. This value is in good agreement with the TEM results shown in Fig. 6.2. However, TEM images also show that the samples are made of particles of different shapes and sizes, from spherical nanoparticles of about 5 nm in size to bigger particles and nanorods of about $3-5$ nm in diameter.

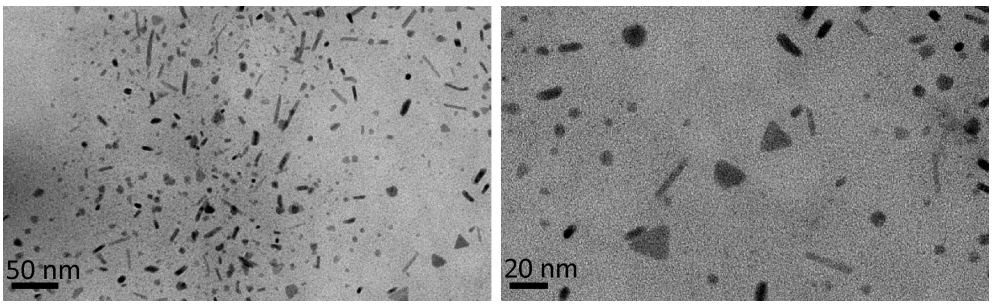

Figure 6.2: TEM images of Yb^{3+}-doped CdS nanocrystals prepared by ball milling.

6.2.2 Optical properties and X-ray diffraction under high pressure

The experimental results of the absorption, Raman and XRD experiments on CdS nanoparticles under high pressure have been analyzed considering only the ZB structure at low pressures, and are presented in this section.

Absorption

Some representative CdS nanocrystals absorption spectra at different pressures are shown in Fig. 6.3. An analysis of the spectra at low pressures indicates that the absorption at the fundamental edge can be described by eq. 2.19. This corresponds to a direct gap transition between parabolic bands, VB and CB, and it is in agreement with the band structure of the metastable ZB structure of CdS at AP [16], [17]. When the pressure is raised above 6 GPa, the CdS nanocrystals suddenly become brown colored, and a large and abrupt red-shift is observed in the absorption edge. Previous high pressure optical studies in bulk CdS indicated an abrupt red-shift in the optical absorption edge at 2.7-3.0 GPa, and this was identified to be due to a first-order W-to-RS phase transition [22], [23]. Moreover, the transition pressure for the ZB-to-RS phase transition was found to be around 8 GPa in CdS colloidal nanocrystals [24]. In this work, the ZB-to-RS phase transition is also observed at pressures much higher than the bulk transition pressure of ca. 3 GPa. This kind of result has been usually observed in nanocrystalline semiconductors systems of the group IV as well as III-V or II-VI in comparison with the bulk counterpart [25]. The high transition pressure can be explained by a higher value of the surface tension for the RS phase nanocrystals compared to the ZB-CdS [6]. An example of the absorption

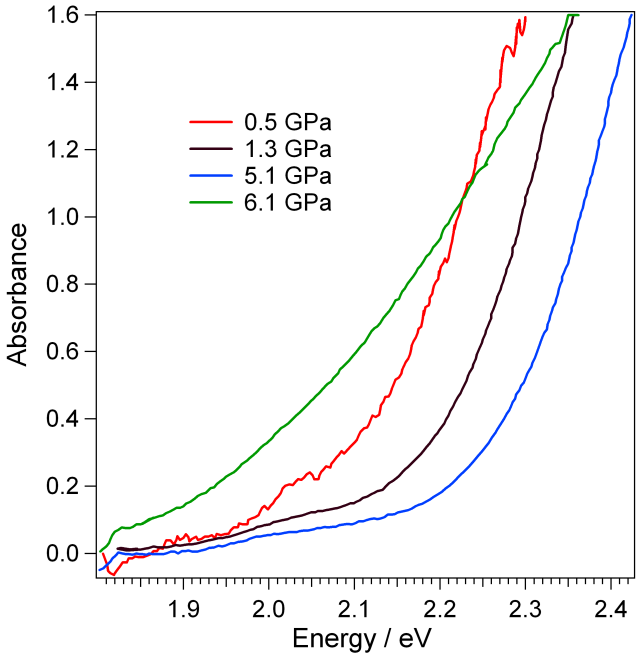

Figure 6.3: Shift in the absorption spectra of CdS nanoparticles with hydrostatic pressure.

edge for the high pressure RS phase recorded at 6.1 GPa is shown in Fig. 6.3. The edge in the RS phase is strikingly different compared to that of CdS nanocrystals in the ZB phase, and is clearly due to an indirect transition.

The ZB-CdS optical energy bandgap values, $E_g^d(\mathrm{ZB})$, have been obtained by extrapolating the square of the absorbance fitting curves, α^2 versus $\hbar\omega$, to $\alpha = 0$. The resulting $E_g^d(\mathrm{ZB})$ pressure dependence is shown in Fig. 6.4, and a blue-shift of the direct bandgap

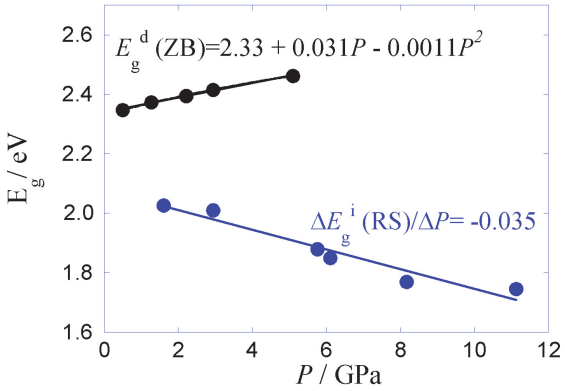

Figure 6.4: Pressure dependence of the optical energy bandgap, E_g, in both ZB and RS structures for CdS nanocrystals.

with pressure is observed. For most semiconductors, the variation of the direct bandgap under pressure can be described by the following quadratic expression [24]:

$$E_g(P) = E_g(0) + aP + bP^2 \tag{6.1}$$

The fit of the experimental data to eq. 6.1 gives the following values: $E_g(0) = 2.33$ eV, $a = 31 \pm 4$ meV/GPa and $b = -1.1 \pm 0.3$ meV/GPa^2. The obtained linear pressure coefficient is lower than the one reported for the direct energy gap for ZB-CdS colloidal nanoparticles, 45.7 meV/GPa [24], and for bulk W-CdS, 45.5 ± 0.5 meV/GPa [23]. In Fig. 6.4, the estimated indirect energy gap in the RS phase, E_g^i(RS), is also plotted as a function of pressure. The E_g^i(RS) values have been obtained from a plot of $\alpha^{1/2}$ versus $\hbar\omega - E_g^i$ and extrapolating the resultant straight line to $\alpha = 0$. The fitted linear pressure dependence is -35 ± 5 meV/GPa. A similar negative shift was observed in II-VI analog semiconductors in the RS phase at high pressure [26]. However, it is very difficult to determine exactly the indirect bandgap of CdS nanoparticles in the high pressure RS phase due to the formation of band-tail states because of the large number of defects and dislocations induced by pressure throughout the phase transitions. The highest pressure achieved in the up-stroke is 11 GPa. Absorption spectra has also been recorded upon releasing pressure down to 1.6 GPa. As observed in Fig. 6.4, the bandgap does not revert to its original value in the ZB phase within this pressure range. This behavior is clearly opposite to the reversible transition with no hysteresis observed in CdS colloidal nanocrystals by Haase and Alivisatos [24].

Raman spectroscopy

The CdS nanoparticles Raman spectra have been studied at RT under hydrostatic pressure up to 7 GPa (Fig. 6.5). The LO and 2LO modes are observed at 304 and 608 cm^{-1} at AP, and shift linearly with pressure to higher energies (see Fig. 6.6(a)) with a pressure coefficient of 4.8 ± 0.2 cm^{-1}/GPa for the LO mode, and 9.2 ± 0.4 cm^{-1}/GPa for the 2LO one, respectively. These slope values are in good agreement with previous results for bulk W-CdS [27], [28] and ZB-CdS colloidal nanocrystals [24]. In addition to these modes, a shoulder is observed overlapping the LO mode, and it has been ascribed to a

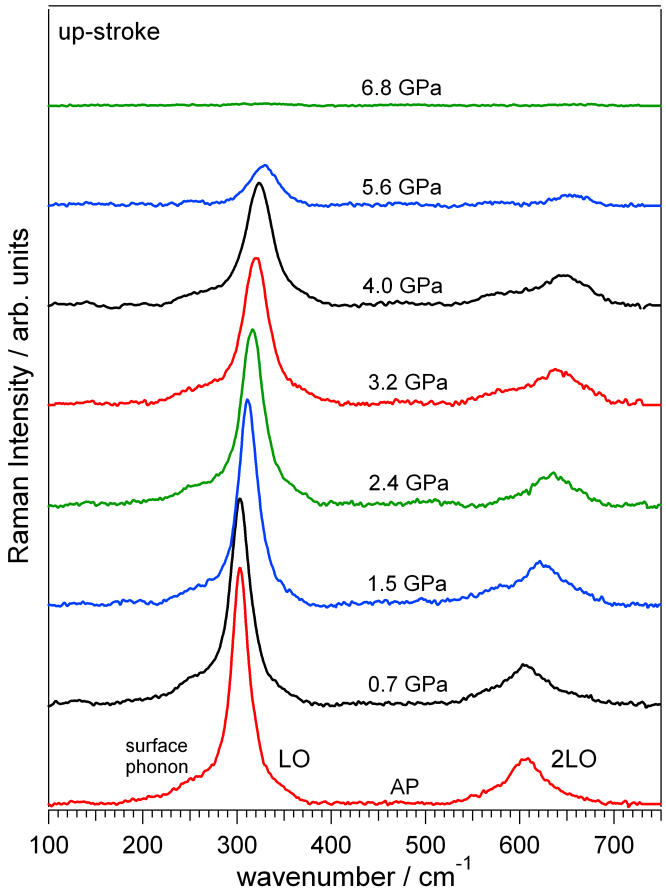

Figure 6.5: RT Raman spectra (λ_{exc} = 514.5 nm) of CdS nanoparticles at different pressures (up-stroke).

surface mode [29]. In nanocrystalline samples the contribution of the surface scattering may be comparable to the volume Raman scattering; Scott and Damen also indicated the observation of surface modes in CdS by Raman spectroscopy [30]. The dependence of the surface mode energy on pressure is shown in Fig. 6.6(b). Above 6.8 GPa the Raman peaks disappears proving the ZB-to-RS CdS nanocrystals phase transition.

The Raman spectra of the CdS nanocrystals have been recorded after the phase transition by decreasing pressure from 8 to 0 GPa. The data are shown in Fig. 6.7(a). It can be seen that no Raman peaks are recovered down to 1.3 GPa and hence, ZB phase remains within this pressure range. Nevertheless, LO and 2LO Raman modes appear again when pressure is released to 0 GPa; therefore, it is concluded that the ZB-to-RS phase transition is reversible although presents a large hysteresis. Figure 6.7(b) compares the CdS nanoparticles Raman spectra at AP before and after the phase transition. The

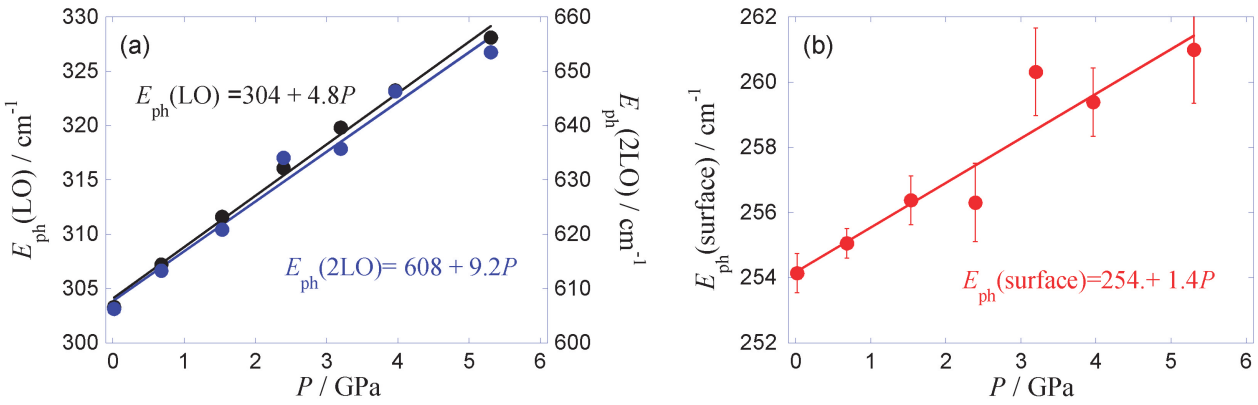

Figure 6.6: Pressure dependence of the energy of the observed phonons, E_{ph}, for CdS nanocrystals. LO and 2LO Raman modes (a), and surface mode (b).

fact that both spectra are centered at the same frequency indicates that no appreciable change in size is induced by the phase transition.

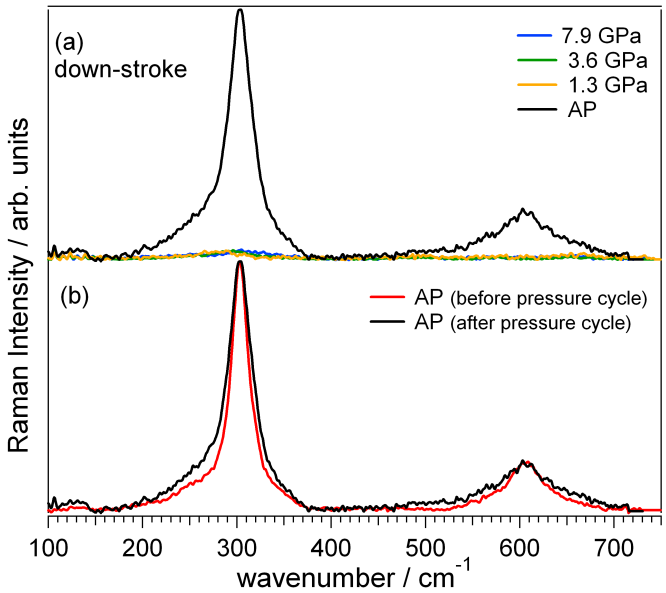

Figure 6.7: RT Raman spectra (λ_{exc} = 514.5 nm) of CdS nanoparticles upon decreasing pressure (a) and comparison between the AP Raman spectra before and after the pressure cycle (b).

The variation of the intensity of LO and 2LO Raman modes with pressure is depicted in Fig. 6.8. An intensity reduction is observed upon increasing pressure. According to the Raman cross-section (eq. 2.10), the peaks intensity should be compensated for possible absorption effects at the bandgap to quantify the real Raman intensity decrease due to the ZB-to-RS phase transition onset. However, since in our particular case the excitation

energy, 2.41 eV (514.5 nm), is close to the bandgap values, the bandgap absorption contribution cannot be estimated.

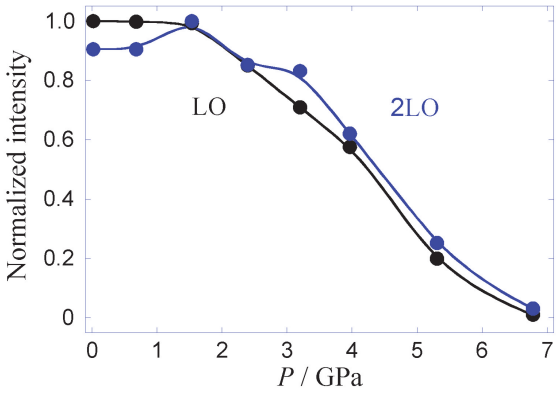

Figure 6.8: Pressure dependence of the normalized intensity of LO and 2LO Raman modes for CdS nanocrystals.

X-ray diffraction

Figure 6.9 shows the evolution of the CdS nanoparticles XRD patterns under high pressure up to 7.5 GPa in both the up and down stroke. It is observed that peaks corresponding to ZB-CdS shift to higher angles with increasing pressure, consistent with a volume decrease. This phase starts to transform into the RS structure at around 4.3 GPa, and both phases coexist between 4.3 and 5.4 GPa. Above this pressure, only the RS structure is observed. The RS phase is maintained during the whole releasing pressure process, and therefore, from XRD experiments we would say that this phase transition is irreversible. Preceding XRD studies showed that bulk W-CdS crystals transformed to the RS structure between 2 and 3 GPa [31], [32].

The cell parameters at different pressures have been determined from the XRD patterns Rietveld refinement. Only ZB and RS phases have been considered before and after the phase transition respectively, while both structures have been included in the fittings during the phases coexistence, between 4.3 and 5.4 GPa. The volume dependence on pressure has been fitted to a Murnaghan equation of state (eq. 2.23) and is depicted in Fig. 6.10. A 7% volume reduction is observed between 0 and 5 GPa, besides, a 15% volume change has been detected at the phase transition.

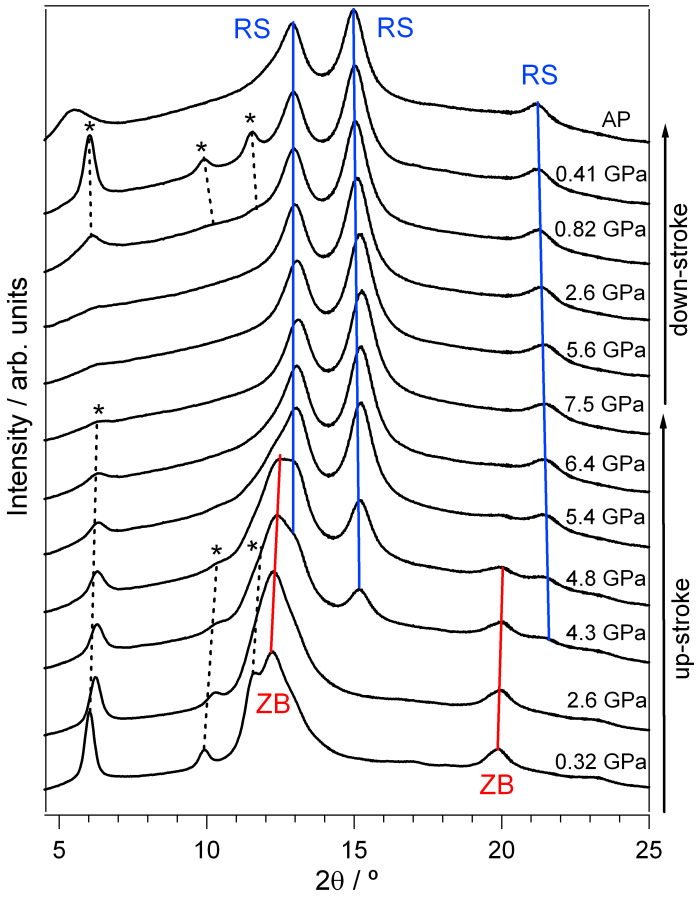

Figure 6.9: XRD patterns of CdS nanoparticles under high pressure. Asterisks represent the diffraction peaks of the hydrostatic medium (silicon oil).

The following bulk modulus values have been obtained by fixing its pressure derivative to $B_0' = 4$; $B_0 = 74 \pm 2$ GPa for the ZB structure, and $B_0 = 107 \pm 5$ GPa for the RS phase. Therefore, the ZB structure is more compressible than the RS one. The bulk modulus values for the CdS single crystals are around 60 GPa in the W phase [32], [33], and ca. 85 GPa in the RS structure [32], [34]. An increase in both the relative volume change at the transition pressure, and the bulk modulus value when decreasing particle size was previously described in Fe_2O_3 nanocrystals [35], or Ag and Au nanoparticles [36], and it was ascribed to surface effects or bond length compression within the particles due to strain effects.

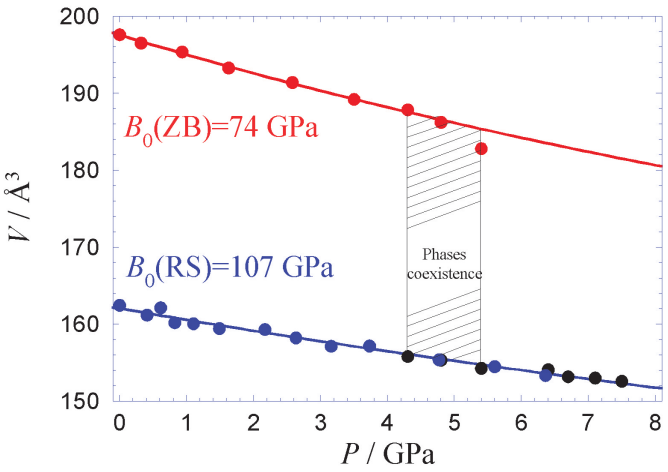

Figure 6.10: Isothermal equation of state of CdS nanoparticles for the ZB (red circles) and RS (black circles in the up-stroke and blue circles in the down-stroke) structures. In both cases the volume dependence on pressure has been fitted to a Murnaghan equation.

6.2.3 Conclusions

CdS nanocrystals in the metastable ZB cubic structure with an average diameter of 5 nm have been prepared in a planetary ball mill. The ZB-to-RS phase transition has been identified by changes in the optical absorption and Raman spectra as well as in the XRD patterns. The direct optical energy gap of ZB-CdS nanoparticles increases with pressure and the value of the linear pressure coefficient is $a = 31 \pm 4$ meV/GPa. When the pressure is raised above 6 GPa, a change from direct to indirect gap occurs. In the RS phase, the pressure dependence of the indirect gap is -35 ± 5 meV/GPa. The energy of LO and 2LO Raman modes for CdS nanoparticles increases with pressure with the same rate as bulk W-CdS. Raman measurements have also evidenced that the ZB-to-RS phase transition for CdS nanocrystals takes place at around 6.0-6.5 GPa, and the fact that the ZB structure is recovered at AP in the down-stroke. XRD measurements under high pressure have shown that ZB-CdS nanoparticles undergo a transition into the RS structure above 5.4 GPa. Bulk modulus of $B_0 = 74 \pm 2$ GPa and $B_0 = 107 \pm 5$ GPa have been obtained for the low-pressure and high-pressure structures, respectively. It has been observed in three different experiments that the stability domain of the ZB structure increases up to 6 GPa at RT for CdS nanocrystals with 5 nm diameter.

6.3 Colloidal nanocrystalline $Zn_{1-x}Co_xO$

6.3.1 Synthesis and characterization

ZnO crystallizes at RT and AP in the W-type structure (hexagonal, $P6_3mc$ space group). This structure is formed from a hexagonal Bravais lattice and a motive of two atoms of each element. The lattice parameters are a_0=3.2495 Å and c_0=5.2069 Å [37]. In an ideal W structure, cations and anions form two compacted interpenetrated hexagonal lattices. Each atom (Zn or O) is tetrahedrally coordinated and occupies sites of C_{3v} symmetry (Fig. 6.11).

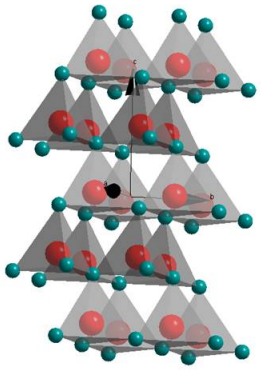

Figure 6.11: $Zn_{1-x}Co_xO$ W structure. The Zn^{2+} (or Co^{2+}) ions (red) are tetrahedrally coordinated by oxygens (green).

The application of hydrostatic pressure to ZnO causes a decrease in the unit cell volume and an increase in the coulomb repulsion. At a given pressure, it becomes energetically favorable for ZnO to assume the more compact RS structure (cubic, $Fm\bar{3}m$ space group). The RS structure may be described by two face-centre-cubic (fcc) lattices shifted by $a/2$, with a_0=4.275 Å. In this case, both atoms (Zn and O) are in an octahedral coordination symmetry (Fig. 6.12). It was demonstrated that on the pressure up-stroke, bulk polycrystalline ZnO undergoes a W-to-RS phase transition at around 9 GPa [38], [39]. On the down-stroke, bulk ZnO was seen to recover its original W structure at either 2 GPa or 4 GPa [39], [40].

The electronic band structure of W-ZnO at RT and AP (Fig. 6.13 left) consists of three broad regions with the CB comprising of Zn 4s levels, the upper VB of O 2p levels and the lower VB of Zn 3d levels. It must be pointed out that the bandgap occurs at Γ

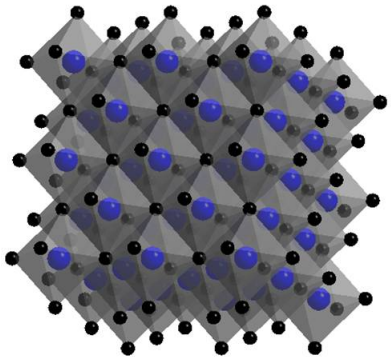

Figure 6.12: $Zn_{1-x}Co_xO$ RS structure. The Zn^{2+} (or Co^{2+}) (blue) are octahedrally coordinated by oxygens (black).

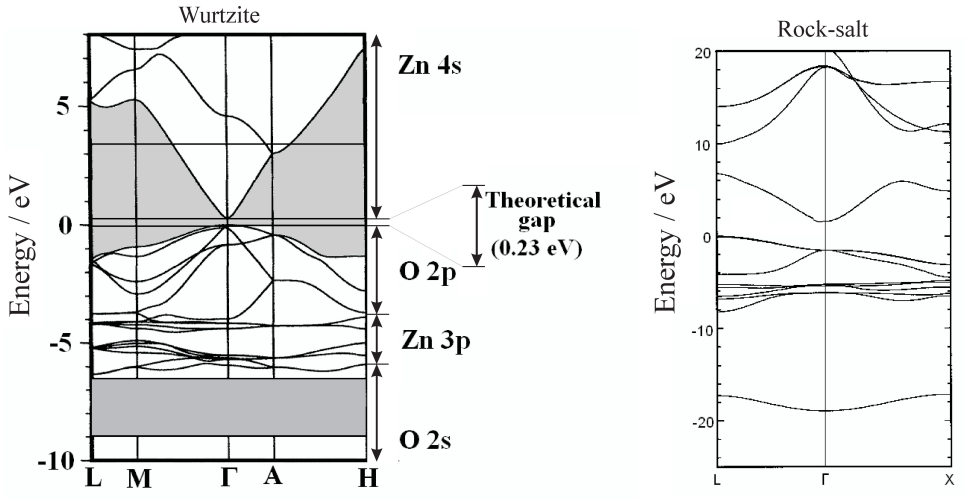

Figure 6.13: Electronic band structure of W-ZnO (left) and RS-ZnO (right) taken from Ref. [43].

and it is a direct transition (E_g = 3.4 eV for bulk ZnO) [41]. The band structure of the RS phase (Fig. 6.13 right) indicates that the interband transition is no longer a direct gap at Γ, but it becomes an indirect gap between L and Γ, with reference to the fcc Brillouin zone [42].

ZnO colloidal nanocrystalline samples doped with different Co^{2+} concentrations have been prepared in this work according to the synthesis methods described in Section 3.7. XRD measurements carried out by M.A. White *et al.* (patterns shown in Fig. 6.14) indicate a good crystallization in the W structure in all cases [14]. The cell parameters obtained for W-ZnO nanoparticles, a=3.2078 Å and c=5.1962 Å, are slightly smaller than the standard bulk values (a_0=3.2495 Å and c_0=5.2069 Å). This lattice contraction with

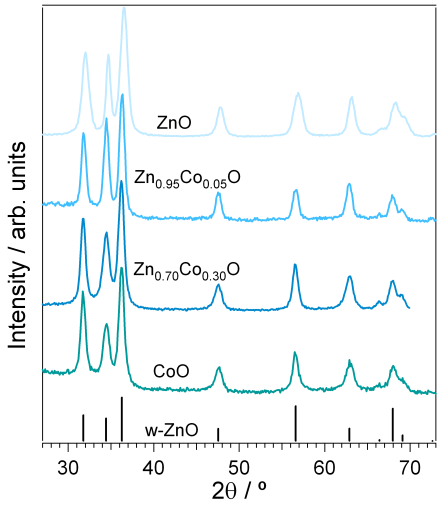

Figure 6.14: XRD patterns of $Zn_{1-x}Co_xO$ colloidal nanocrystals carried out by M.A. White, Univ. of Washington. The calculated pattern for W-ZnO is also shown.

decreasing particle size was previously observed in metallic nanoparticles [44].

TEM images of ZnO: 5%Co^{2+} colloidal nanocrystals (Fig. 6.15) show spherical nanoparticles with an average particle diameter of ca. 4 nm. This size is around four times larger than the size of the bulk exciton (0.9 nm), and therefore, we are again in the weak confinement regime [45]. A narrow size distribution for the W-$Zn_{1-x}Co_xO$ nanoparticles prepared by this method was previously demonstrated by D.A. Schwartz *et al.* [46].

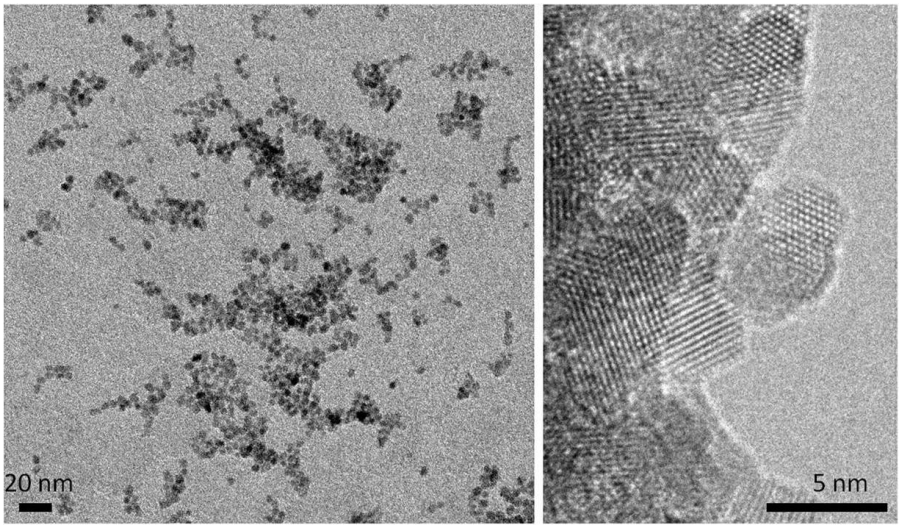

Figure 6.15: TEM and HRTEM images of ZnO: 5%Co^{2+} nanoparticles.

6.3.2 Optical properties under high pressure

In this work, the RT electronic structure of W-$Zn_{1-x}Co_xO$ nanoparticles has been investigated by means of optical absorption and Raman spectroscopy under pressure.

Absorption

- **ZnO**

  Figure 6.16 shows the pressure dependence of the ZnO nanoparticles (average size 4 nm) absorption spectra up to 24 GPa. A monotonous blue-shift of the absorption edge is observed as pressure increases. Since the optical absorption edge in W-ZnO colloidal nanocrystals is caused by direct absorption, it remains sharp with increasing pressure, and its pressure dependence can be determined accurately according to eq. 2.19. When the pressure is raised above 14 GPa, the W-to-RS phase transition occurs, and the absorption edge changes dramatically compared to lower pressures. Both direct and indirect energy gaps are observed for ZnO nanocrystals in the RS structure. Although it is much more difficult in this case, the RS-ZnO indirect energy gap can also be estimated from eq. 2.22.

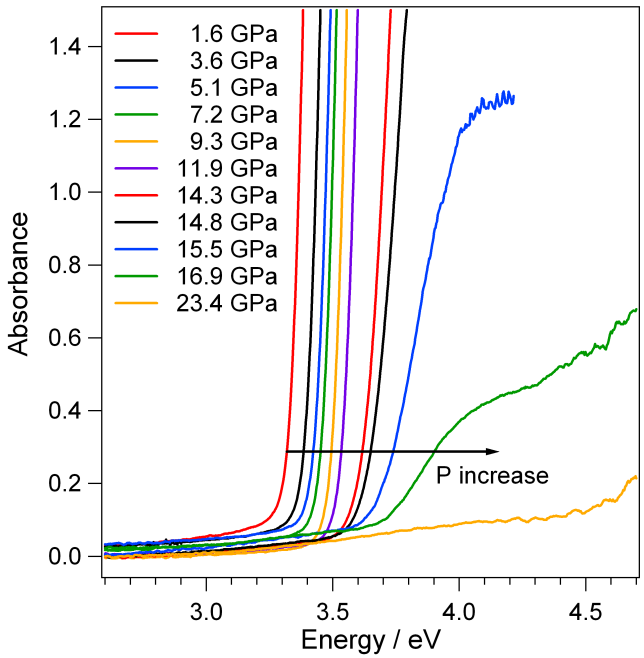

Figure 6.16: Absorption spectra of ZnO nanocrystals (ca. 4 nm) upon increasing pressure.

In previous absorption experiments, an increase in the energy bandgap with pressure was noted for both ZnO bulk crystals and thin films, and the W $\rightarrow$ RS phase transition was observed at around 9.5 GPa [42], [47]. The phase transition in ZnO thin films was detected as a decrease in the absorbance at the edge. Since RS-ZnO is an indirect gap semiconductor with low absorption coefficient, only intense direct absorption edges were detectable in transmission measurements in a 200 nm thick film [47]. The transition from the W-ZnO bulk sample to the RS phase was observed as a neat change in the shape of the absorbance [42]. An intense transition at energies higher than 4.5 eV in both RS-ZnO bulk and films was also assigned to an allowed direct transition [42], [47]. High pressure synchrotron XRD experiments indicated the transition pressure to be around 10.5 GPa for W-ZnO with 50 nm in diameter, and 15 GPa for 12 nm nanocrystalline ZnO [48], [49]. Grzanka *et al.* also studied the size effect on the high pressure phase transition of ZnO nanocrystals, obtaining similar results [50]. Shan *et al.* studied the pressure dependence of the luminescence properties in ZnO nanowires and they found the phase transition at around 12 GPa [51]. But, as far as we know, no experimental investigations on the optical absorption of ZnO nanocrystals under high pressure have been reported so far.

Figure 6.17(a) compares the variation with pressure of the direct optical energy gap in W-ZnO colloidal nanocrystals, $E_g^d(W)$, with the relative pressure dependence of the total energy gap for the high pressure RS structure, $\Delta E_g^{d+i}(RS)$. $E_g^d(W)$ values have been obtained from the fitting of the square of the absorbance to eq. 2.19, α^2-$\hbar\omega$, $E_g^d(W)$ being the point at which the absorption fitting curve goes to zero. The variation with pressure of both direct and indirect contributions to the absorption edge in the RS phase, $\Delta E_g^{d+i}(RS)$, has been estimated considering the value of the energy at a fixed absorbance for each pressure. In Fig. 6.17(b) the pressure dependence of the indirect optical energy gap for the ZnO nanoparticles in the RS structure, $E_g^i(RS)$, is shown. $E_g^i(RS)$ values are obtained as follows: $\alpha^{1/2}$ is plotted versus $\hbar\omega$, and the $\hbar\omega$ value at $\alpha = 0$ is equal to $E_g^i + \hbar\Omega$; where $\hbar\Omega$ is the phonon energy, estimated to be ca. 55 meV (438.4 cm^{-1}) from Raman measurements.

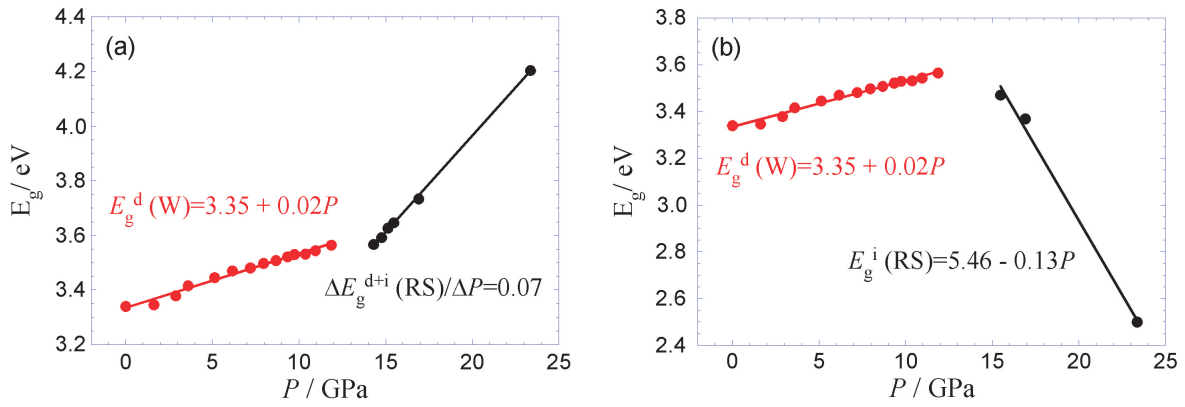

Figure 6.17: Pressure dependence of the ZnO direct energy gap in the W phase, E_g^d, and both direct and indirect gaps in the RS structure, ΔE_g^{d+i}, (a). And pressure dependence of the direct gap for W-ZnO, E_g^d, and indirect gap for RS-ZnO, E_g^i (b).

The pressure coefficient for the W-ZnO nanoparticles direct absorption edge is 20 ± 2 meV/GPa (Fig. 6.17). This value is slightly lower than the one measured in W-ZnO bulk (25 ± 2 meV/GPa) and thin film (23.0 ± 0.5 meV/GPa) [47]. For ZnO colloidal nanocrystals in the RS structure, the relative variation of the total energy gap with pressure is given by 70 ± 1 meV/GPa (Fig. 6.17(a)). It can be seen that the direct energy gap increases with pressure while the indirect one decreases with a pressure coefficient given by -130 ± 10 meV/GPa (Fig. 6.17(b)).

Absorption spectra of ZnO nanoparticles recorded in the down-stroke between 20 and 1 GPa are shown in Fig. 6.18. They indicate the non-reversibility of the W-to-RS phase transition, that is, the metastability of RS-ZnO nanocrystals after the pressure cycle. However, since AP has not been reached, a complete certainty of the RS phase stability does not exist for the pure ZnO nanocrystalline sample. High pressure structural investigations of bulk ZnO indicated that the W-to-RS transition is reversible at RT; with a transition pressure of 9 GPa upon increasing pressure and 2 GPa in the down-stroke [39]. However, this property was already demonstrated to be drastically different for nanocrystals, and Decremps *et al.* showed that metastable RS ZnO nanoparticles were obtained upon decreasing pressure after a high-pressure (15 GPa) and high-temperature (550 K) treatment [52].

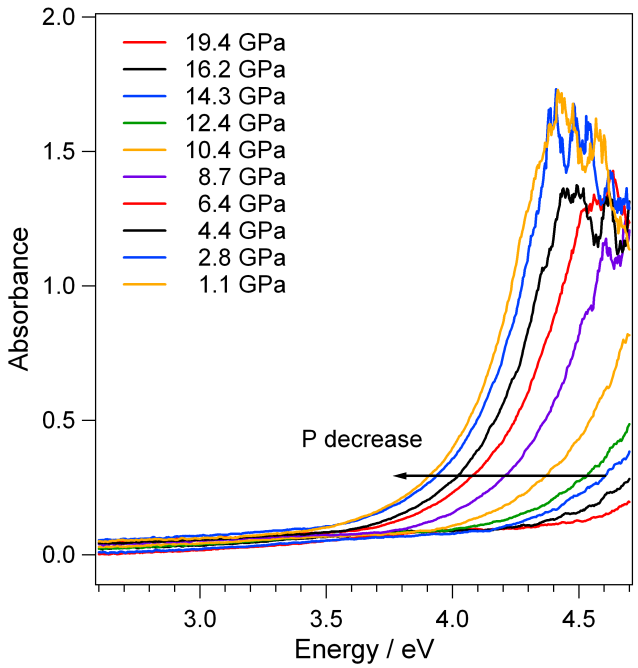

Figure 6.18: Absorption edge of RS-ZnO nanoparticles at different pressures (down-stroke).

- **ZnO: 5%Co^{2+}**

  Bandgap absorption spectra of ZnO: 5%Co^{2+} nanoparticles for different pressures up to 20 GPa are shown in Fig. 6.19. The dependence of the Co^{2+} absorption bands upon increasing pressure is presented in Fig. 6.20. Figure 6.21 compares the bandgap absorption in pure and 5%Co^{2+}-doped ZnO nanocrystals. Absorption spectra of $Zn_{1-x}Co_xO$ nanocrystals present three main differences with respect to pure W-ZnO which are summarized in Fig. 6.22 [53]:

  - The energy of the fundamental band-to-band absorption edge is slightly red-shifted.
  - A broad band absorption, related to a charge-transfer transition involving promotion of an electron from the Co^{2+} to the CB, appears at energies just below (and overlapping) the band-to-band edge [54].
  - A well defined absorption band related to the spin-allowed $^4A_2 \rightarrow {}^4T_1$ d−d transition of tetrahedral Co^{2+} is observed in the visible region [55].

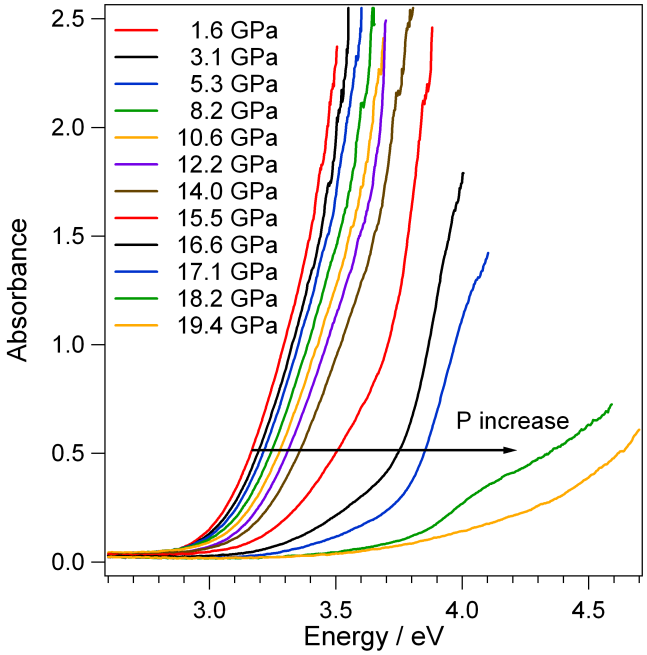

Figure 6.19: Absorption edge of ZnO: 5%Co^{2+} nanoparticles at different pressures (up-stroke).

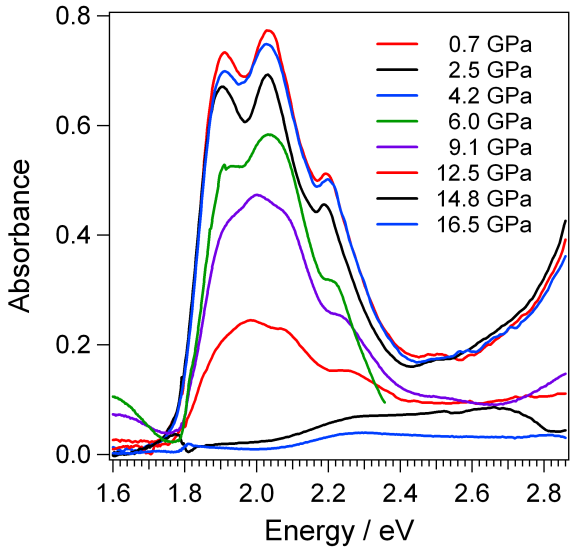

Figure 6.20: RT pressure dependence of the $^4A_2 \rightarrow {}^4T_1$ Co^{2+} transition of ZnO: 5%Co^{2+} nanocrystals.

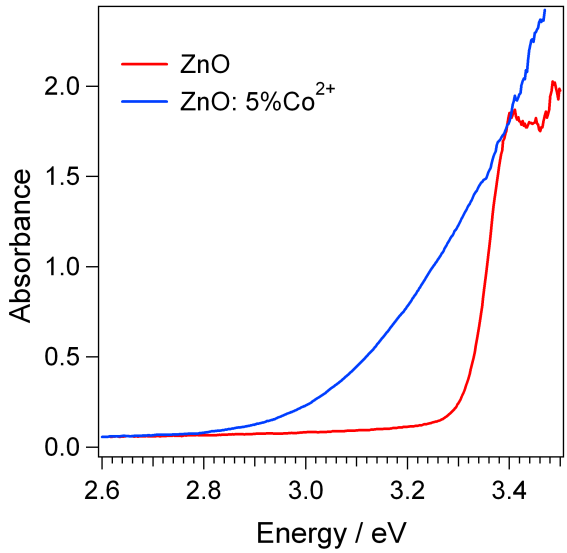

Figure 6.21: Absorption edge of W-ZnO and W-ZnO: 5%Co^{2+} nanoparticles at AP.

An increase of the sample transparency inside the DAC is detected upon increasing pressure, and the W-ZnO: 5%Co^{2+} transition to the RS phase is gradually observed up to 15 GPa in the three absorption features:

- The fundamental absorption edge shifts to higher photon energies, and a change of the absorption edge, when moving from direct to indirect gap scenario, is observed.
- The charge-transfer band virtually disappears, or overlaps the direct transition of the RS phase.
- The d−d Co^{2+} absorption band around 2 eV decreases its intensity by a factor of 10 and shifts to higher energies, 2.5 eV, as a consequence of the modification from a tetrahedral (W phase) to an octahedral (RS phase) coordination symmetry.

Figure 6.23(a) shows the pressure dependence of the ZnO: 5%Co^{2+} nanocrystals optical energy gap for the W and RS structures. Since the charge-transfer band overlaps the bandgap absorption, the direct energy gap in the W phase, E_g^d(W), has been estimated from the fitting of the square of the absorbance to eq. 2.19 like for pure ZnO, but considering only values of the absorbance above 1.5. ΔE_g^{d+i}(RS) has

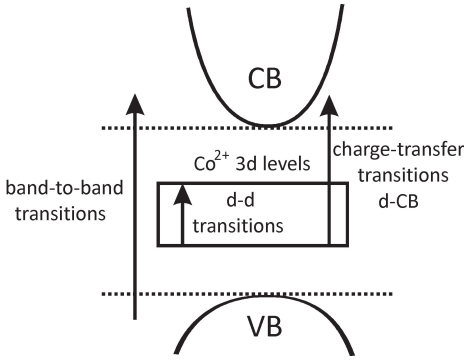

Figure 6.22: Schematic representation of the optical transitions observed in ZnO: 5%Co^{2+}.

been obtained from the value of the energy at a fixed absorbance for each pressure in the RS phase. In Fig. 6.23(b) the pressure dependence of the Co^{2+} normalized absorption intensity is presented. The direct bandgap for the W-ZnO: 5%Co^{2+} nanocrystals exhibits a linear pressure dependence with a pressure coefficient of 17 ± 2 meV/GPa (Fig. 6.23(a)). This value is lower than the one obtained in W-ZnO: 5%Co^{2+} thin films (24.9 meV/GPa) [53].

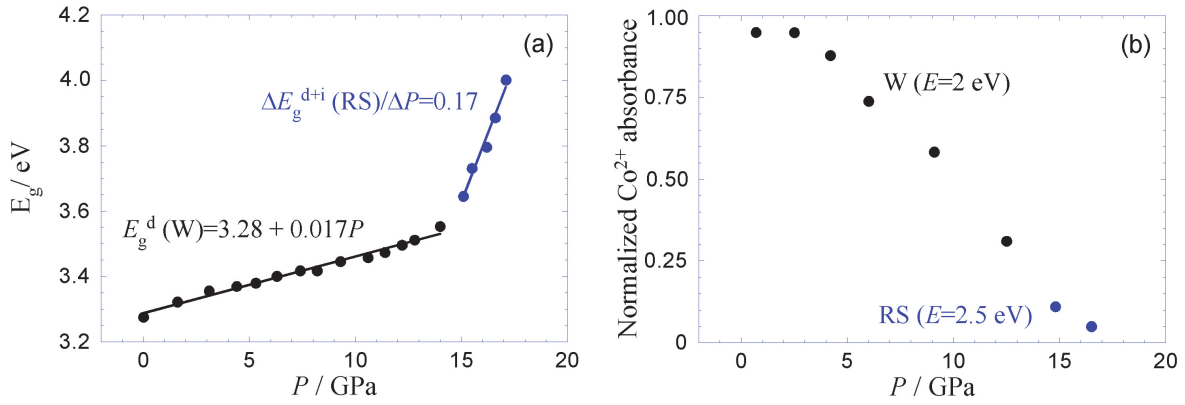

Figure 6.23: Pressure dependence of the ZnO: 5%Co^{2+} direct energy gap in the W phase, E_g^d, and both direct and indirect gaps in the RS structure, ΔE_g^{d+i}, (a). And pressure dependence of the normalized Co^{2+} absorbance (b).

From Figs. 6.20 and 6.23(b) it is clearly seen that the Co^{2+} absorption intensity decreases continuously, which indicates that the W-to-RS phase transition takes place gradually, starting at pressures as low as 4-5 GPa. This result is opposite to the large and abrupt decrease in the Co^{2+} absorption intensity observed in ZnO: Co^{2+} single crystal by Stephens *et al.* [56]. The dramatic change of the absorption

edge detected in $Zn_{1-x}Co_xO$ thin films was used to propose also a sudden W-to-RS phase transition [53]. Nevertheless, it can be deduced from our experimental results (see Fig. 6.23) that the pressure dependence of the bandgap absorption do not provide information about the abrupt or continuous character of the transition. The charge-transfer band absorbance diminution is correlated with the d−d Co^{2+} bands behavior.

The continuous character of the phase transition in ZnO: Co^{2+} nanocrystals evidences that different nanoparticles within our sample present different transition pressures, and this could be attributed to several reasons. Firstly, it could be due to a broad size distribution, since it is well known that the transition pressure increases for smaller particle size [4], [5]. However, this is not the case, as there are nanoparticles which show the phase transition at 4 GPa, while the transition pressure is 9 GPa for the bulk. Secondly, different orientation or morphology of the particles would give rise to differences in the surface energy among the various nanoparticles, and the stability under high pressure is very related to it [25]. Thirdly, if Co^{2+} ions are heterogeneously distributed within our nanocrystalline sample, those nanoparticles with higher cobalt concentration would have higher absorbance and lower transition pressures, involving a decrease in the total absorbance. The W-to-RS phase transition was observed in CoO nanoparticles (around 50 nm in size) in the 0.8-6.9 GPa pressure range by means of high pressure synchrotron-radiation XRD measurements [57].

Several experiments can be accomplished in order to clarify the actual explanation for the gradual phase transition observed in ZnO: Co^{2+} nanoparticles. A concentration study may be carried out on different particles at the TEM facility. Moreover, electron diffraction experiments would give information about the structure of different particles. Hence, the following relevant experiment will be developed: Both concentration and electron diffraction measurements will be performed on ZnO: Co^{2+} nanocrystals after reaching an intermediate pressure in the up-stroke in order to check if the nanoparticles with high Co^{2+} concentration have already undergone

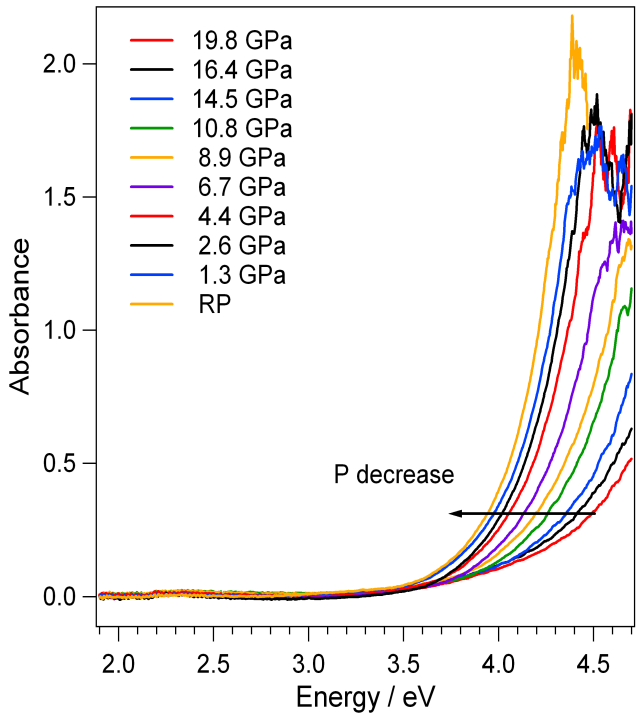

Figure 6.24: Absorption edge of RS-ZnO: 5%Co^{2+} nanoparticles in the down-stroke from 22 GPa to AP.

the phase transition, while those with low Co^{2+} concentration are still in the W phase.

Absorption spectra of ZnO: 5%Co^{2+} nanoparticles recorded after the phase transition, in the down-stroke down to AP are shown in Fig. 6.24. Both the absorption edge at AP (Fig. 6.24) which is characteristic of an indirect semiconductor, and the fact that Co^{2+} tetrahedral absorption is not recovered at AP, are clear evidences of the metastability of the RS-ZnO: 5%Co^{2+} phase at RT and AP.

Raman spectroscopy

The optical phonons predicted for the W-ZnO at the Γ-point of the Brillouin zone are: $\Gamma_{opt} = A_1 + 2B_1 + E_1 + 2E_2$. Both A_1 and E_1 polar modes are Raman and IR active and split into longitudinal and transverse optical (LO and TO) components. The two non-polar E_2^{Low} and E_2^{High} modes are Raman active and IR inactive, while the B_1 silent modes are Raman and IR inactive [58], [59]. The mode assignment for W-ZnO single crystals at RT and AP was well established by Calleja and Cardona [60]. The phonon

confinement of ZnO nanocrystals affects both the phonon energy and the symmetry. A red-shift in both E_2^{Low} and E_2^{High} modes as well as an asymmetric broadening on the low energy side were observed in the Raman spectrum of ZnO nanoparticles (with 17 nm in size) [61].

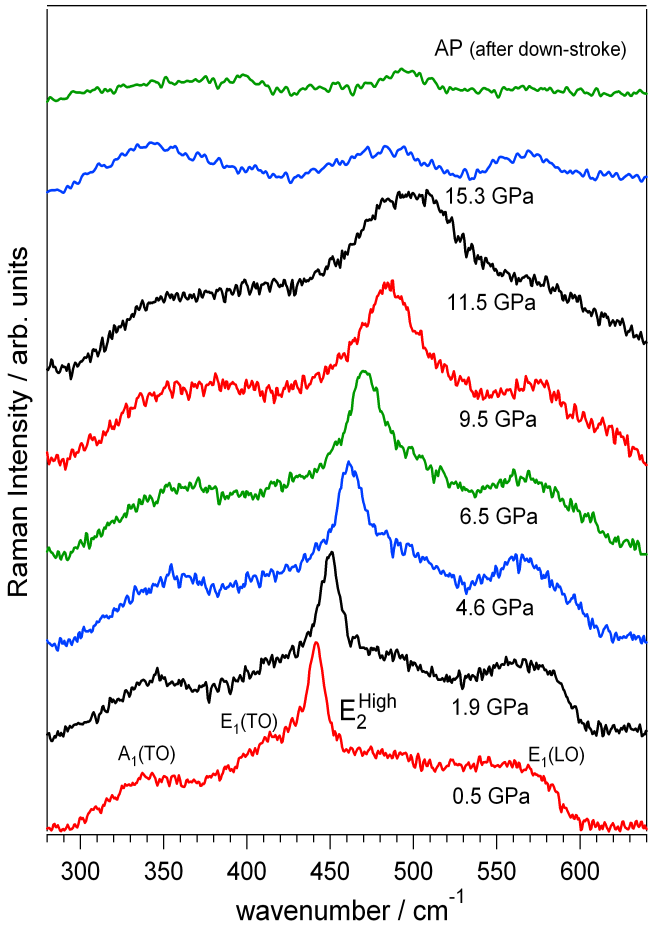

Figure 6.25: Raman spectra of ZnO: 5%Co^{2+} nanoparticles at different representative hydrostatic pressures.

In previous works, the experimental phonon energies at ambient conditions for the E_2^{Low} and E_2^{High} modes were determined to be ca. 100 and 440 cm^{-1}, respectively, for both W-ZnO and W-ZnO: 5%Co^{2+} single crystals. The A_1(TO), E_1(TO) and E_1(LO) modes were also clearly seen in the Raman spectra at around 380, 414 and 580 cm^{-1}, respectively. On the contrary, the A_1(LO) mode was not observed. Moreover, additional lines in the ZnO: 5%Co^{2+} spectra were attributed to CoO magnetic excitations [58], [59], [60]. Raman scattering measurements performed by Decremps *et al.* in bulk ZnO also

evidenced a W-to-RS structural transformation at around 9 GPa [59]. High pressure Raman spectra of ZnO nanowires showed a reversible W-to-RS phase transition with transition pressures of 10.3 GPa in the up-stroke and 4.4 GPa in the down-stroke [62].

The pressure dependence of the zone-center phonons (E_2, A_1 and E_1) has been measured in this work for the W-ZnO: 5%Co^{2+} nanoparticles and is shown in Fig. 6.25. The E_2^{High} mode is prominently observed in the spectra while the other modes are hardly observable and then could only be tentatively assigned. The hexagonal to cubic phase transition is completed around 15 GPa for the W-ZnO: 5%Co^{2+} nanocrystals (ca. 4 nm in size). Contrary to bandgap absorption but similarly to Co^{2+} absorption, Raman measurements may give information concerning whether the phase transition is abrupt or continuous. Figure 6.26(a) shows the pressure dependence of the intensity of the E_2^{High} Raman mode. In order to determine the Raman intensity decrease due to the W-to-RS structural phase transition onset, the intensity must be corrected for absorption effects at the bandgap. Considering the Raman cross-section (eq. 2.10), and the fact that the energy bandgap, 3.28 eV, separates from the excitation energy, 2.41 eV (514.5 nm), at a rate of 17 meV/GPa, the compensated E_2^{High} intensity variation with pressure is depicted in Fig. 6.26(b). A decrease of the intensity with increasing pressure is clearly detected below 5 GPa, which points out the gradual character of the W-to-RS phase transition in ZnO: 5%Co^{2+} nanoparticles.

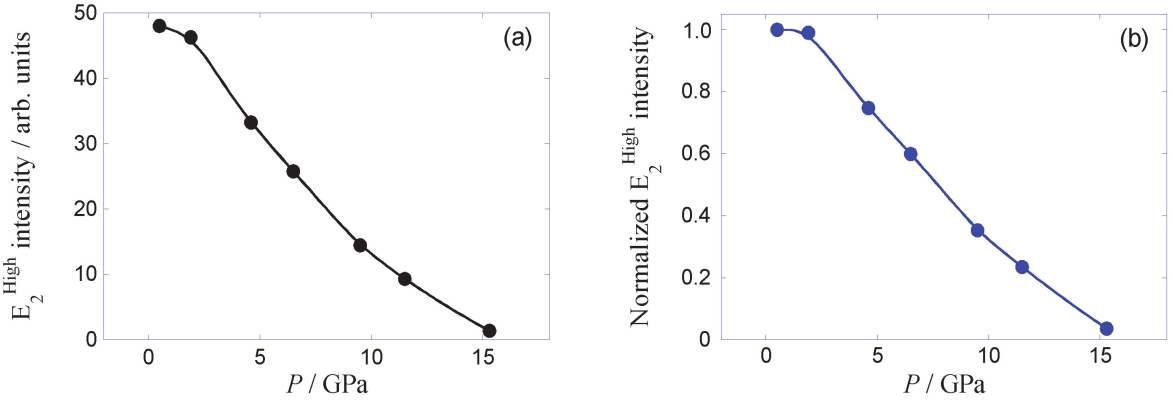

Figure 6.26: Pressure dependence of the E_2^{High} experimental intensity (a) and normalized corrected intensity (see text) (b) for ZnO: 5%Co^{2+} nanocrystals.

The pressure dependence of the E_2^{High} phonon energy up to the W→RS phase transition

is shown in Fig. 6.27 and has been fitted to a second-order polynomial [63]:

$$\omega = \omega(0) + aP + bP^2 \tag{6.2}$$

with $\omega(0) = 438.4$ cm^{-1}, $a = 6.0 \pm 0.2$ cm^{-1}/GPa and $b = 0.17 \pm 0.03$ cm^{-1}/GPa^2. The experimental wavenumber at AP obtained in this work for the ZnO: 5%Co^{2+} nanocrystals, 438.4 cm^{-1}, is evidently red-shifted compared to the different bulk values, 444 cm^{-1} or 440 cm^{-1} given in the literature [27], [59]. This result is attributed to a relaxation of the momentum conservation, and it confirms the confinement effect [61]. The linear frequency dependence of E_2^{High}, $a = 6.0 \pm 0.2$ cm^{-1}/GPa, is similar to the value reported for W-ZnO single crystal, 5.2 cm^{-1}/GPa [59]. Above the transition pressure no active Raman modes are observed. As it can be seen in Fig. 6.25, the studied nanoparticles remain in the RS phase after the pressure down-stroke. Hence, Raman measurements also indicate the metastability of the RS-ZnO: 5%Co^{2+} nanocrystals at ambient pressure.

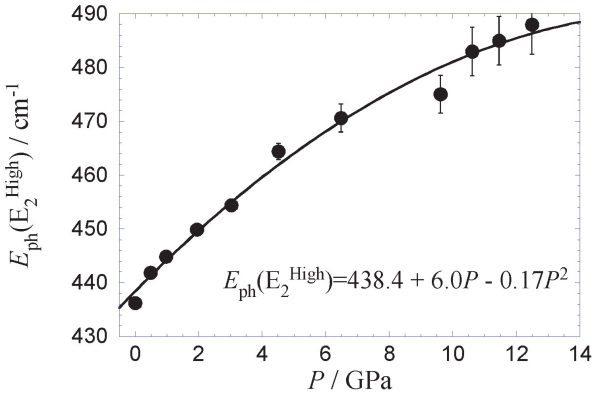

Figure 6.27: Pressure dependence of the E_2^{High} optical phonon energy, E_{ph}, for W-ZnO: 5%Co^{2+} nanoparticles.

6.3.3 Conclusions

The irreversible phase transition of W-ZnO and W-ZnO: 5%Co^{2+} colloidal nanocrystals (4 nm in size) to the RS structure has been demonstrated by absorption and Raman measurements. The ZnO nanoparticles direct absorption spectra have been measured as a function of pressure showing a blue-shift (20 ± 2 meV/GPa) of the optical bandgap

with pressure up to 14 GPa, where the W-to-RS phase transition takes place. Absorption spectra recorded upon decreasing pressure indicate the metastability of the RS-ZnO nanoparticles. Besides the bandgap absorption, the spectra of ZnO: 5%Co^{2+} nanocrystals present a charge-transfer band and an absorption band due to Co^{2+} absorption in a tetrahedral coordination. In this sample, the phase transition is gradually observed and completed at around 14 GPa. This result is opposite to the abrupt transition detected in ZnO: Co^{2+} single crystals and thin-films, and it is not fully understood yet. The absorption spectra during the down-stroke evidence the metastability of RS-ZnO: 5%Co^{2+} nanoparticles at RT and AP. The pressure dependence of the ZnO: 5%Co^{2+} E_2^{High} Raman mode also shows that the W-to-RS phase transition is completed at ca. 15 GPa, and that ZnO: 5%Co^{2+} nanocrystals remain in the RS structure at AP.

Bibliography

[1] Q. Jiang, C.C. Yang, and J.C. Li. Melting enthalpy depression of nanocrystals. *Mater. Lett.*, **56**: 1019–1021, 2002.

[2] S. Xiao, W. Hu, and J. Yang. Melting Behaviors of Nanocrystalline Ag. *J. Phys. Chem. B*, **109**: 20339–20342, 2005.

[3] S.H. Tolbert and A.P. Alivisatos. High−Pressure Structural Transformations in Semiconductor Nanocrystals. *Annu. Rev. Phys. Chem.*, **46**: 595425, 1995.

[4] S.M. Clark, S.G. Prilliman, C.K. Erdonmez, and A.P. Alivisatos. Size dependence of the pressure-induced γ to α structural phase transition in iron oxide nanocrystals. *Nanotech.*, **16**: 2813–2818, 2005.

[5] S.H. Tolbert and A.P. Alivisatos. Size Dependence of a First Order Solid-Solid Phase Transition: The Wurtzite to Rock-Salt Transformation in CdSe Nanocrystals. *Science*, **265**: 373–376, 1994.

[6] K. Jacobs, D. Zaziski, E.C. Scher, A.B. Herhold, and A.P. Alivisatos. Activation Volumes for Solid-Solid Transformations in Nanocrystals. *Science*, **293**: 1803–1806, 2001.

[7] M. Bruchez Jr, M. Moronne, P. Gin, S. Weiss, and A.P. Alivisatos. Semiconductor Nanocrystals as Fluorescent Biological Labels. *Science*, **281**: 2013–2016, 1998.

[8] A.H. Mueller, M.A. Petruska, M. Achermann, D.J. Werder, E.A. Akhadov, D.D. Koleske, M.A. Hoffbauer, and V.I. Klimov. Multicolor Light-Emitting Diodes Based on Semiconductor Nanocrystals Encapsulated in GaN Charge Injection Layers. *Nano Lett.*, **5**: 10391044, 2005.

[9] C. Ricolleau, L. Audinet, M. Gandais, and T. Gacoin. Structural transformations in II-VI semiconductor nanocrystals. *Eur. Phys. J. D*, **9**: 565–570, 1999.

[10] J.M.D. Coey. Dilute magnetic oxides. *Curr. Opin. Solid State Mater. Sci.*, **10**: 83–92, 2006.

[11] H. Ohno, D. Chiba, F. Matsukura, T. Omiya, E. Abe, T. Dietl, Y. Ohno, and K. Ohtani. Electric-field control of ferromagnetism. *Nature*, **408**: 944–946, 2000.

[12] K. Sato and H. Katayama-Yoshida. Electronic structure and ferromagnetism of transition-metal-impurity-doped zinc oxide. *Physica B*, **308-310**: 904–907, 2001.

[13] K. Ueda, H. Tabata, and T. Kawai. Magnetic and electric properties of transition-metal-doped ZnO films. *Appl. Phys. Lett.*, **79**: 988–990, 2001.

[14] M.A. White, S.T. Ochsenbein, and D.R. Gamelin. Colloidal Nanocrystals of Wurtzite $Zn_{1-x}Co_xO$ $(0 \leqslant x \leqslant 1)$: Models of Spinodal Decomposition in an Oxide Diluted Magnetic Semiconductor. *Chem. Mater.*, **20**: 7107–7116, 2008.

[15] M.G. Bawendi, A.R. Kortan, M.L. Steigerwald, and L.E. Brus. X-ray structural characterization of larger CdSe semiconductor clusters. *J. Chem. Phys.*, **91**: 7282–7290, 1989.

[16] M. Cardona and G. Harbeke. Optical Properties and Band Structure of Wurtzite-Type Crystals and Rutile. *Phys. Rev.*, **137**: A1467–A1476, 1965.

[17] K.J. Chang, S. Froyen, and M.L. Cohen. Electronic band structures for zinc-blende and wurtzite CdS. *Phys. Rev. B*, **28**: 4736–4743, 1983.

[18] H.S. Nalwa, editor. *Handbook of Nanostructured Materials and Nanotechnology*. Academic Press, New York, 2000.

[19] R.W.G. Wyckoff, editor. *Crystal Structures*, volume 2. John Wiley and Sons, New York, London, 1963.

[20] Y.N. Xu and W.Y. Ching. Electronic, optical, and structural properties of some wurtzite crystals. *Phys. Rev. B*, **48**: 4335–4351, 1993.

[21] C. Kumpf, R.B. Neder, F. Niederdraenk, P. Luczak, A. Stahl, M. Scheuermann, S. Joshi, S.K. Kulkarni, C. Barglik-Chory, C. Heske, and E. Umbach. Structure determination of CdS and ZnS nanoparticles: Direct modeling of synchrotron-radiation diffraction data. *J. Chem. Phys.*, **123**: 224707–1–224707–6, 2005.

[22] A.L. Edwards and H.G. Drickamer. Effect of Pressure on the Absorption Edges of Some III-V, II-VI, and I-VII Compounds. *Phys. Rev.*, **122**: 1149–1157, 1961.

[23] B. Batlogg, A. Jayaraman, J.E. Van Cleve, and R.G. Maines. Optical absorption, resistivity, and phase transformation in CdS at high pressure. *Phys. Rev. B*, **27**: 3920–3923, 1983.

[24] M. Haase and A.P. Alivisatos. Arrested solid-solid phase transition in 4-nm-diameter cadmium sulfide nanocrystals. *J. Phys. Chem.*, **96**: 6756–6762, 1992.

[25] A. San-Miguel. Nanomaterials under high-pressure. *Chem. Soc. Rev.*, **35**: 876–889, 2006.

[26] J. Gonzalez, F.V. Perez, E. Moya, and J.C. Chervin. Hydrostatic Pressure Dependence of the Energy Gaps of CdTe in the Zinc-Blende and Rocksalt Phases. *J. Phys. Chem. Solids*, **56**: 335–340, 1995.

[27] C.A. Arguello, D.L. Rousseau, and S.P.S. Porto. First-Order Raman Effect in Wurtzite-Type Crystals. *Phys. Rev.*, **181**: 1351–1363, 1969.

[28] U. Venkateswaran, M. Chandrasekhar, and H.R. Chandrasekhar. Luminescence and Raman spectra of CdS under hydrostatic pressure. *Phys. Rev. B*, **30**: 3316–3319, 1984.

[29] M. Abdulkbadar and B. Thomas. Study of Raman spectra of nanoparticles of CdS and ZnS. *Nanostruct. Mater.*, **5**: 289–298, 1995.

[30] J.F. Scott and T.C. Damen. Raman scattering from surface modes of small CdS crystallites. *Optics Communications*, **5**: 410–412, 1972.

[31] N.B. Owen, P.L. Smith, J.E. Martin, and A.J. Wright. X-ray Diffraction at ultra-high pressures. *J. Phys. Chem. Solids*, **24**: 1519–1524, 1963.

[32] H. Sowa. On the mechanism of the pressure-induced wurtzite- to NaCl-type phase transition in CdS: an X-ray diffraction study. *Solid State Sci.*, **7**: 73–78, 2005.

[33] G.A. Samara and A.A. Giardini. Compressibility and Electrical Conductivity of Cadmium Sulfide at High Pressures. *Phys. Rev.*, **140**: A388–A395, 1965.

[34] T. Suzuki, T. Yagi, S. Akimoto, T. Kawamura, S. Toyoda, and S. Endo. Compression behavior of CdS and BP up to 68 GPa. *J. Appl. Phys.*, **54**: 748–751, 1983.

[35] J.Z. Jiang, J.S. Olsen, L. Gerward, and S. Mørup. Enhanced bulk modulus and reduced transition pressure in $\gamma-Fe_2O_3$ nanocrystals. *Europhys. Lett.*, **44**: 620–626, 1998.

[36] Q.F. Gu, G. Krauss, W. Steurer, F. Gramm, and A. Cervellino. Unexpected High Stiffness of Ag and Au Nanoparticles. *Phys. Rev. lett.*, **100**: 045502, 2008.

[37] R. Heller, J. McGannon, and A. Weber. *J. Appl. Phys.*, **21**: 1283, 1950.

[38] C.H. Bates, W.B. White, and R. Roy. New High-Pressure Polymorph of Zinc Oxide. *Science*, **137**: 993, 1962.

[39] S. Desgreniers. High-density phases of ZnO: Structural and compressive parameters. *Phys. Rev. B*, **58**: 14102, 1998.

[40] F.J. Manjón, K. Syassen, and R. Lauck. Effect of Pressure on Phonon Modes in Wurtzite Zinc Oxide. *High Press. Res.*, **22**: 299–304, 2002.

[41] D. Vogel, P. Krüger, and J. Pollmann. Ab initio electronic-structure calculations for II-VI semiconductors using self-interaction-corrected pseudopotentials. *Phys. Rev. B*, **52**: R14316–R14319, 1995.

[42] A. Segura, J.A. Sans, F.J. Manjón, A. Munoz, and M.J. Herrera-Cabrera. Optical properties and electronic structure of rock-salt ZnO under pressure. *Appl. Phys. Lett.*, **83**: 278–280, 2003.

[43] S.J. Gilliland. *Structural, Optical and Magnetic Characterization of Pulsed Laser Deposited Thin Films of $Zn_{1-x}M_xO$ (M=Mn, Fe, Ni, Cu) Transparent Magnetic Alloys.* PhD thesis, University of Valencia, 2008.

[44] G. Apai, J.F. Hamilton, J. Stohr, and A. Thompson. Extended X-Ray Absorption Fine Structure of Small Cu and Ni Clusters: Binding-Energy and Bond-Length Changes with Cluster Size. *Phys. Rev. Lett.*, **43**: 165–169, 1979.

[45] V.A. Fonoberov and A.A. Balandin. Radiative lifetime of excitons in ZnO nanocrystals: The dead-layer effect. *Phys. Rev. B*, **70**: 195410, 2004.

[46] D.A. Schwartz, N.S. Norberg, Q.P. Nguyen, J.M. Parker, and D.R. Gamelin. Magnetic Quantum Dots: Synthesis, Spectroscopy, and Magnetism of Co^{2+}- and Ni^{2+}-doped ZnO Nanocrystals. *J. Am. Chem. Soc.*, **125**: 13205–13218, 2003.

[47] J.A. Sans, A. Segura, F.J. Manjón, B. Marí, A. Munoz, and M.J. Herrera-Cabrera. Optical properties of wurtzite and rock-salt ZnO under pressure. *Microelectronics Journal*, **36**: 928–932, 2005.

[48] R.S. Kumar, A.L. Cornelius, and M.F. Nicol. Structure of nanocrystalline ZnO up to 85 GPa. *Curr. Appl. Phys.*, **7**: 135–138, 2007.

[49] J.Z. Jiang, J.S. Olsen, L. Gerward, D. Frost, D. Rubie, and J. Peyronneau. Structural stability in nanocrystalline ZnO. *Europhys. Lett.*, **50**: 48–53, 2000.

[50] E. Grzanka, S. Gierlotka, S. Stelmakh, B. Palosz, T. Strachowski, A. Swiderska-Sroda, G. Kalisz, W. Lojkowski, and F. Porsch. Phase transition in nanocrystalline ZnO. *Z. Kristallogr. Suppl.*, **23**: 337–342, 2006.

[51] W. Shan, W. Walukiewicz, J.W. Ager III, K.M. Yu, Y. Zhang, S.S. Mao, R. Kling, C. Kirchner, and A. Waag. Pressure-dependent photoluminescence study of ZnO nanowires. *Appl. Phys. Lett.*, **86**: 153117, 2005.

[52] F. Decremps, J. Pellicer-Porres, F. Datchi, J.P. Itié, A. Polian, F. Baudelet, and J.Z. Jiang. Trapping of cubic ZnO nanocrystallites at ambient conditions. *Appl. Phys. Lett.*, **81**: 4820–4822, 2002.

[53] J.A. Sans, A. Segura, J.F. Sánchez-Royo, Ch. Ferrer-Roca, and E. Guillotel. Pressure dependence of the optical properties of wurtzite and rock-salt $Zn_{1-x}Co_xO$ thin films. *phys. stat. sol. (b)*, **244**: 407–412, 2007.

[54] S.G. Gilliland, J.A. Sans, J.F. Sánchez-Royo, G. Almonacid, and A. Segura. Charge-transfer absorption band in $Zn_{1-x}M_xO$ (M: Co, Mn) investigated by means of photoconductivity, Ga doping, and optical measurements under pressure. *Appl. Phys. Lett.*, **96**: 241902, 2010.

[55] P. Koidl. Optical absorption of Co^{2+} in ZnO. *Phys. Rev. B*, **15**: 2493–2499, 1977.

[56] D.R. Stephens and H.G. Drickamer. Effect of Pressure on Tetrahedral Ni^{++} and Co^{++} Complexes. *J. Chem. Phys.*, **35**: 429–435, 1961.

[57] J.F. Liu, Y. He, W. Chen, G.Q. Zhang, Y.W. Zeng, T. Kikegawa, and J.Z. Jiang. Bulk Modulus and Structural Phase Transitions of Wurtzite CoO Nanocrystals. *J. Phys. Chem. C*, **111**: 2–5, 2007.

[58] M. Millot, J. González, I. Molina, B. Salas, Z. Golacki, J.M. Broto, H. Rakoto, and M. Goiran. Raman spectroscopy and magnetic properties of bulk ZnO: Co single crystal. *J. Alloy Compd.*, **423**: 224–227, 2006.

[59] F. Decremps, J. Pellicer-Porres, A.M. Saitta, J.C. Chervin, and A. Polian. High-pressure Raman spectroscopy study of wurtzite ZnO. *Phys. Rev. B*, **65**: 092101, 2002.

[60] J.M. Calleja and M. Cardona. Resonant Raman scattering in ZnO. *Phys. Rev. B*, **16**: 3753–3761, 1977.

[61] J. Marquina, Ch. Power, and J. González. Raman scattering on ZnO nanocrystals. *Rev. Mex. Fis.*, **53**: 170–173, 2007.

[62] X. Yan, Y. Gu, X. Zhang, Y. Huang, J. Qi, Y. Zhang, T. Fujita, and M. Chen. Doping Effect on High-Pressure Structural Stability of ZnO Nanowires. *J. Phys. Chem. C*, **113**: 1164–1167, 2009.

[63] J. González, B.J. Fernández, J.M. Besson, M. Gauthier, and A. Polian. High-pressure behaviour of Raman modes in $CuGaS_2$. *Phys. Rev. B*, **46**: 15092–15101, 1992.